Local Thermometry of Neutral Modes on the Quantum Hall Edge

Local Thermometry of Neutral Modes on the Quantum Hall Edge

Vivek Venkatachalam[†1], Sean Hart[†1], Loren Pfeiffer[2], Ken West[2], Amir Yacoby[1]

[1]Department of Physics, Harvard University, Cambridge, MA, USA
[2] Department of Electrical Engineering, Princeton University, Princeton, NJ, USA
[†]These authors contributed equally to this work

Summary: Quantum dots, used as local thermometers, detect upstream heat transport in a $\nu = 2/3$ fractional quantum Hall edge state, even when the state is carrying no net charge.

Abstract

A system of electrons in two dimensions and strong magnetic fields can be tuned to create a gapped 2D system with one dimensional channels along the edge. Interactions among these edge modes can lead to independent transport of charge and heat, even in opposite directions. Measuring the chirality and transport properties of these charge and heat modes can reveal otherwise hidden structure in the edge. Here, we heat the outer edge of such a quantum Hall system using a quantum point contact. By placing quantum dots upstream and downstream along the edge of the heater, we can measure both the chemical potential and temperature of that edge to study charge and heat transport, respectively. We find that charge is transported exclusively downstream, but heat can be transported upstream when the edge has additional structure related to fractional quantum Hall physics.

When a two-dimensional electron system (2DES) is subject to a strong perpendicular magnetic field and tuned such that the ratio of electrons to magnetic flux quanta in the system (ν) is near certain integer or fractional values, the bulk of the system develops a gap due to either quantization of kinetic energy (the integer quantum Hall, or IQH, effect) or strong correlations arising from non-perturbative Coulomb interactions (the fractional quantum Hall, or FQH, effect) [1]. While the bulk (2D) is gapped and incompressible, the edge (1D) of the system contains compressible regions with gapless excitations that carry charge chirally around the system, in a direction determined by the external magnetic field. Compressible edge states have gained more attention recently due to their ability to serve as a bus for quasiparticles that exist in exotic FQH phases[2, 3]. These edges, however, can have considerable internal structure that is not apparent from bulk transport measurements.

The spatial structure of edges is dictated by the interplay between the external confining potential which defines the edge, an additional harmonic confinement from the magnetic field, and Coulomb interactions. It was predicted [4] and verified [5, 6, 7] that for a smooth, topgate-defined confining potential, it is energetically favorable for the electron density to redistribute slightly to create alternating compressible and incompressible strips. This has the effect of spatially separating edges corresponding to different filling factors. Such an effect is not present in sharper edges [8].

Perhaps more surprising than this spatial structure is the possibility of modes that carry energy (or heat) upstream, even as the magnetic field carries the injected charge downstream. The edge of the $\nu = 2/3$ FQH state was originally predicted to consist of a $\nu = 1$ edge of electrons going downstream with a $\nu = 1/3$ edge of holes going upstream [9, 10]. However, this edge structure would suggest a two-terminal conductance of $G_{2T} = \frac{4}{3}\frac{e^2}{h}$. Scattering between the edges would lead to non-universal values in the range of $\frac{2}{3}\frac{e^2}{h} \leq G_{2T} \leq \frac{4}{3}\frac{e^2}{h}$. Experimentally, however, no such two terminal conductance has been measured. Direct approaches to look for upstream charge transport in the time domain have similarly turned up no evidence [11]. This motivated a picture in which disorder induces scattering and equilibration between the edges, forcing the charge to travel exclusively downstream. Heat, however,

would be allowed to travel diffusively upstream and downstream, leading to a nonzero thermal Hall conductivity and partial upstream heat transport at $\nu = 2/3$ [12, 13].

Evidence for upstream heat transport in a $\nu = 2/3$ edge was recently obtained by performing modified shot noise measurements [14]. Our approach studies the same state by directly placing thermometers upstream and downstream of a current-source heater to observe charge and heat transport along the edge.

As our heater, we use a lithographically fabricated quantum point contact (QPC), tuned to the tunneling regime (Fig. 1C). Tunneling of electrons through this QPC at elevated energy locally excites the outermost compressible component of a gate-defined edge. We then place quantum dots 20 μm upstream and downstream of the QPC to measure charge and heat transport (Fig. 1A). The edge itself is defined by a separate pair of gates (green in Fig. 1A), and the perpendicular magnetic field defines a clockwise charge-propagation direction (with respect to Figure 1). All measurements were carried out in a dilution refrigerator with a minimum electron temperature of 20 mK, measured with Coulomb blockade thermometry.

To first characterize the structure of the edge that we are tunneling charge into, we energize a subset of gates upstream (blue) and downstream (red) of the central QPC to create additional point contacts that serve as imperfect voltage probes ($R \sim 100$ kΩ). This ensures that we only measure the chemical potential of the outermost edge component [15]. Current is injected through the central QPC (10 pA sourced through O3 and drained at O6). The upstream chemical potential, $V1 - V7$, was observed to be immeasurably small in all measurements, indicating that no charge is transported upstream on a 20 μm scale. The downstream chemical potential, $V5 - V7$, can be used to determine the resistance of the edge connecting the source to the probe (the "local Hall" resistance R_L). This resistance is plotted in blue in Figure 2. Additional measurement details can be found in the online supplement.

For magnetic fields (B) between 2 T and 8 T, the measured value $R_L = 1\frac{h}{e^2}$ indicates that the charge is carried between the injector and detector by electronic modes that behave similarly to an IQH $\nu = 1$ edge. Inner edges can (and must, at fields below 6 T) be present, as can be seen by comparing R_{xy} with R_L. These inner edges, however, do not carry any of the injected charge. Above 8 T, we find that R_L is quantized to $R_L = \frac{2}{3}\frac{h}{e^2}$ even though the bulk is at $\nu = 1$[16]. This suggests that the edge has additional structure consisting of alternating compressible and incompressible regions which are spatially separated, as indicated in Figure 2 (IV). In this situation, we only access the outermost edge of the incompressible $\nu = 2/3$ strip located outside the $\nu = 1$ bulk. The robust quantization that we observe indicates that no charge leaks out of this outermost $\nu = 2/3$ edge over the 20 μm separating the injector from the detector.

The edge-deflecting gates (green in Figure 1A) can be deenergized to deflect the edges into floating ohmic contacts located 250 μm away (O2 and O4), where they will chemically equilibrate and thermally cool (though some equilibration and cooling may occur before the edges reach the ohmic contacts). If we repeat this charge transport measurement with the deflector gates deenergized, we continue to monitor no upstream charge transport. However, the downstream resistance is observed to match exactly the bulk value of R_{xy}, plotted in black in Figure 2. This indicates that our deflection process does, indeed, force all edges to fully chemically equilibrate in ohmic contacts O2 and O4, providing an important control for the heat transport measurements discussed below.

To characterize heat transport, we energize all of the gates upstream and downstream of the central QPC to form quantum dots, which serve as thermometers to measure the temperature of the edge. This is similar to another recent spectroscopic approach [17, 18, 19]. The width of the Coulomb blockade peak as a function of gate voltage can be translated into the temperature of the leads (Fig. 1B, details in SOM A).

With the thermometers active, we inject current through the QPC set to an average transmission of 15% to create a non-equilibrium population in the outermost edge (Fig. 1C). The low transmission ensures that we inject solely electrons into the edge (no FQH edges are fully transmitted). These energetic electrons, however, are not necessarily the elementary excitations of the edge and will therefore excite the natural edge modes as they decompose. By increasing the bias across the QPC, we vary the current (and therefore the power) being delivered to the edge. We monitor both the chemical potential and temperature of the edge at the upstream and downstream dots (Fig. 1B and 1D).

Measurements are first performed with the deflector gates energized, to measure heat transport

associated with the edge (red and blue curves in rows 1 and 2 of Fig. 3). We then repeat the procedure with the deflector gates off, to measure any background heating not associated with the edge (cyan and magenta curves in rows 1 and 2 of Fig. 3). The difference between these two temperatures gives us a measure of the excess heat carried by the edge (bottom row in Fig. 3, red is downstream and blue is upstream temperature).

At the two lowest fields that were measured (2.41 T and 3.8 T), our charge transport measurements indicate that we are injecting charge into a $\nu = 1$ edge sitting outside an incompressible bulk at filling $\nu = 3$ or $\nu = 2$ respectively. This is depicted schematically in Fig. 2 (I,II) and in Fig. 4 (II). By monitoring the chemical potential as we vary the injected power, we find that charge is carried exclusively by the outermost $\nu = 1$ edge over the entire range of measurement (SOM A).

At 2.41 T, when the bulk is at $\nu = 3$, there is no measurable background heating either upstream or downstream. When the deflectors are turned on, we find heating downstream but none upstream. When the bulk is at $\nu = 2$, we find about 2-3 mK of background heating that is perfectly cancelled in the upstream direction. Thus, in both cases, we find that heat carried by edge modes is transported exclusively downstream. While this strict downstream heat transport in the IQH regime is expected and matches previous measurements [20, 14], surprisingly, the magnitude of the temperature observed does not agree with what one would expect from quantized thermal transport (assuming an equilibrated edge):

$$K_H \equiv \frac{\partial J_E}{\partial T} = n\frac{\pi^2}{3}\frac{k_B^2}{h}T \implies T = \frac{\sqrt{6hJ_E/n}}{\pi k_B},$$

where J_E is the power carried by the edge and n is the number of IQH edges participating in transport [13]. At $\nu = 2$, for an injected power of 350 fW, we expect an edge temperature between 430 mK and 608 mK, depending on how well the two edges thermally equilibrate ($n = 2$ or $n = 1$). Our measured temperature of 30 mK indicates that a substantial quantity of heat is transferred out of the edge[18]. We can model the behavior of heat transport for out-of-equilibrium Fermi systems (SOM B), which indicates a similar temperature deficiency. Both models, however, give the correct shape for the temperature versus power curves presented in Figure 3.

At the highest measured field, 8.3 T, charge transport (Fig. 2) indicates that we have an incompressible $\nu = 2/3$ strip outside a $\nu = 1$ bulk, depicted schematically in Fig. 2 (IV). Here we see substantially more background heating, both upstream and downstream, but after subtracting contributions from the bulk (deflectors energized) we still find an upstream temperature rise of 5 mK at 300 fW, compared to a downstream rise of 11 mK. Such upstream heating is consistent with the predicted diffusive conductivity of the outer $\nu = 2/3$ edge[13], though the assymmetry between upstream and downstream temperatures suggests that the inner $\nu = 1 \to 2/3$ edge (which carries heat preferentially downstream) is partially participating in heat transport.

At the second highest measured field, 6.2 T, one would expect, based on charge transport, behavior similar to what we find when the bulk is at $\nu = 2$ or $\nu = 3$, with all heat being carried downstream by the integer $\nu = 1$ edge. Instead, we find behavior similar to what was observed at 8.3 T, with heating both upstream and downstream and a slight asymmetry between the two. This surprising result can be understood if we allow for the presence additional structure in the $\nu = 1$ edge that does not affect charge transport. Perhaps the simplest such structure would be the presence of an incompressible strip of $\nu = 2/3$, much like what we see at 8.3 T, but with charge equilibrating between the two separated edges of this strip (Fig. 2 (III)). With these edges equilibrated, we measure a local Hall resistance of $R_L = \frac{h}{e^2}$. However, the diffusive heat transport provided by the outer $\nu = 2/3$ edge could still carry heat to the upstream thermometer (edge IV in Fig. 4). Additional evidence for such an edge structure is presented in SOM D. Importantly, this mechanism of upstream heating by an apparent $\nu = 1$ edge would not be universal and would depend sensitively on the spatial reconstruction of that edge. A sharper mesa-defined edge with a larger density gradient [20, 14] or a lower-mobility 2DES may not allow an incompressible strip of $\nu = 2/3$ to form outside the $\nu = 1$ bulk. In the online supplement (SOM D), we present a device with a mesa-defined edge that shows no upstream heat transport at 6.2 T (edge III in Fig. 4).

By studying the charge and heat transport properties of the outermost component of a gate-defined quantum Hall edge, these measurements paint a picture in which such edges contain considerable struc-

ture. Charge transport along the edge shows that correlated FQH modes can exist outside an IQH bulk. Even when these charge signatures are not present (Fig. 2 (III) and edge IV in Fig. 4), heat transport suggests that density reconstructions can still create additional edge components that carry heat upstream. In addition to this, by separating bulk and edge contributions, we have been able to observe bulk heat transport at $\nu = 1$ which is absent at $\nu = 2$ and $\nu = 3$, the origin of which remains an open question.

More generally, our system provides a framework to extract quantitative information about charge and heat transport at the boundary of any two-dimensional topological insulator. Such a system can be essential to discriminate between topological states of matter that have identical charge transport behavior. For example, with the $\nu = 5/2$ FQH state, the presence or absence of these neutral modes would allow us to discriminate between distinct ground states that are particle-hole conjugates of each other [21, 22].

References

[1] S. Girvin, R. Prange, *The Quantum Hall Effect* (Springer, 1987).

[2] A. Stern, B. I. Halperin, *Phys. Rev. Lett.* **96**, 016802 (2006).

[3] P. Bonderson, A. Kitaev, K. Shtengel, *Phys. Rev. Lett.* **96**, 016803 (2006).

[4] D. B. Chklovskii, B. I. Shklovskii, L. I. Glazman, *Phys. Rev. B* **46**, 4026 (1992).

[5] N. B. Zhitenev, R. J. Haug, K. v. Klitzing, K. Eberl, *Phys. Rev. Lett.* **71**, 2292 (1993).

[6] S. W. Hwang, D. C. Tsui, M. Shayegan, *Phys. Rev. B* **48**, 8161 (1993).

[7] A. Yacoby, H. Hess, T. Fulton, L. Pfeiffer, K. West, *Solid State Communications* **111**, 1 (1999).

[8] M. Huber, *et al.*, *Phys. Rev. Lett.* **94**, 016805 (2005).

[9] A. H. MacDonald, *Phys. Rev. Lett.* **64**, 220 (1990).

[10] X. G. Wen, *Phys. Rev. Lett.* **64**, 2206 (1990).

[11] R. C. Ashoori, H. L. Stormer, L. N. Pfeiffer, K. W. Baldwin, K. West, *Phys. Rev. B* **45**, 3894 (1992).

[12] C. L. Kane, M. P. A. Fisher, J. Polchinski, *Phys. Rev. Lett.* **72**, 4129 (1994).

[13] C. L. Kane, M. P. A. Fisher, *Phys. Rev. B* **55**, 15832 (1997).

[14] A. Bid, *et al.*, *Nature* **466**, 585 (2010).

[15] B. J. van Wees, *et al.*, *Phys. Rev. Lett.* **62**, 1181 (1989).

[16] L. P. Kouwenhoven, *et al.*, *Phys. Rev. Lett.* **64**, 685 (1990).

[17] C. Altimiras, *et al.*, *Nature Physics* **6**, 34 (2009).

[18] C. Altimiras, *et al.*, *Phys. Rev. Lett.* **105**, 226804 (2010).

[19] S. Takei, M. Milletarì, B. Rosenow, *Phys. Rev. B* **82**, 041306 (2010).

[20] G. Granger, J. P. Eisenstein, J. L. Reno, *Phys. Rev. Lett.* **102**, 086803 (2009).

[21] S.-S. Lee, S. Ryu, C. Nayak, M. P. A. Fisher, *Phys. Rev. Lett.* **99**, 236807 (2007).

[22] M. Levin, B. I. Halperin, B. Rosenow, *Phys. Rev. Lett.* **99**, 236806 (2007).

Acknowledgments: We acknowledge financial support from Microsoft Corporation Project Q, the NSF GRFP, and the DOE SCGF Program.

Author Contributions: V.V. and S.H. conceived and designed the experiments, prepared samples, carried out the experiments and data analysis and wrote the paper. A.Y. conceived and designed the experiments, carried out data analysis and wrote the paper. L.N.P. and K.W.W. carried out the molecular beam epitaxy growth.

Author Information: The authors declare no competing financial interests. Correspondence and requests for materials should be addressed to yacoby@physics.harvard.edu.

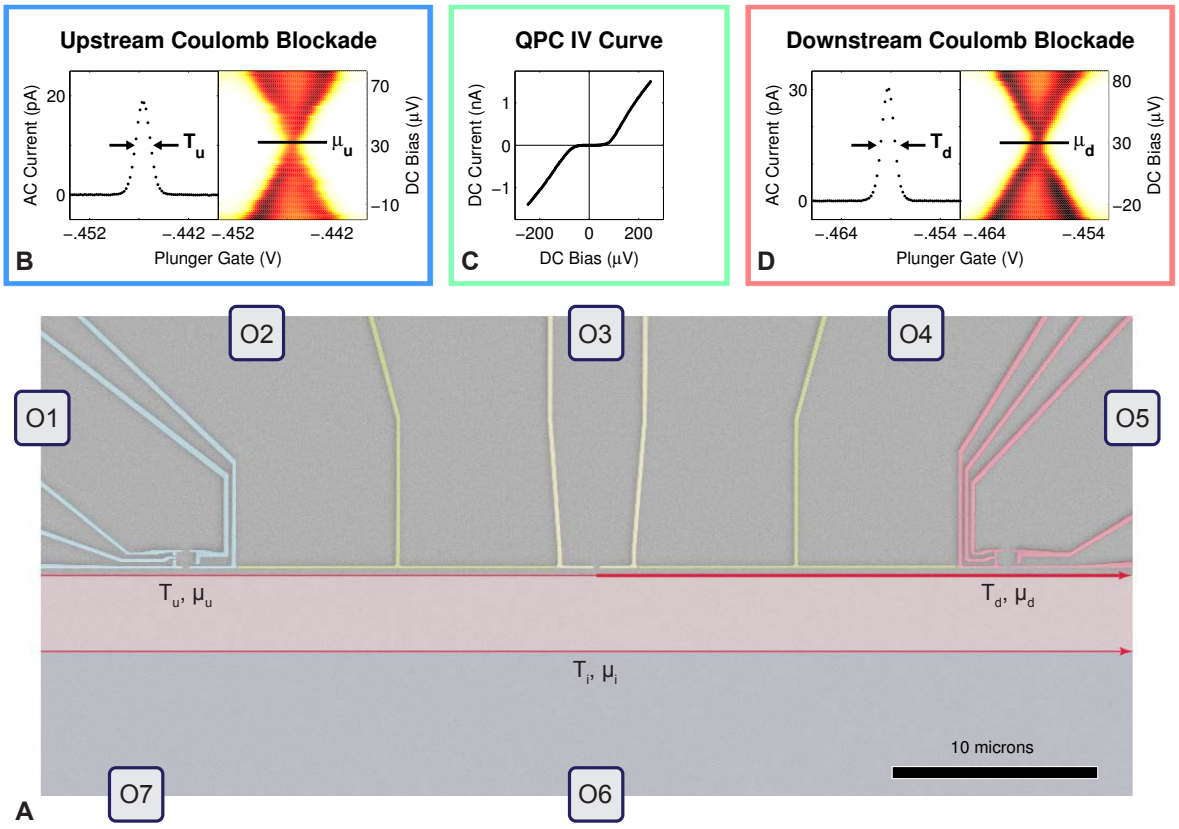

Figure 1: A) Scanning electron micrograph showing the gate geometry of the device. O1-7 denote ohmic contacts. Injection of current through the central quantum point contact (QPC) populates the outermost quantum Hall edge channel, creating a non-equilibrium distribution. Deflector gates adjacent to the injection site define the edge or can be de-energized to deflect edge channels to floating ohmic contacts (O2 and O4). A quantum dot located 20 microns downstream of the injection site is used to measure the temperature T_d and chemical potential μ_d of the outer edge channel. Similarly, an upstream dot measures T_u and μ_u. B, D) Coulomb blockade (CB) peaks and diamonds for the quantum dots. The temperature is determined from the CB peak width. The chemical potential is determined by zeroing the voltage bias across the quantum dot. C) The IV characteristic of the QPC.

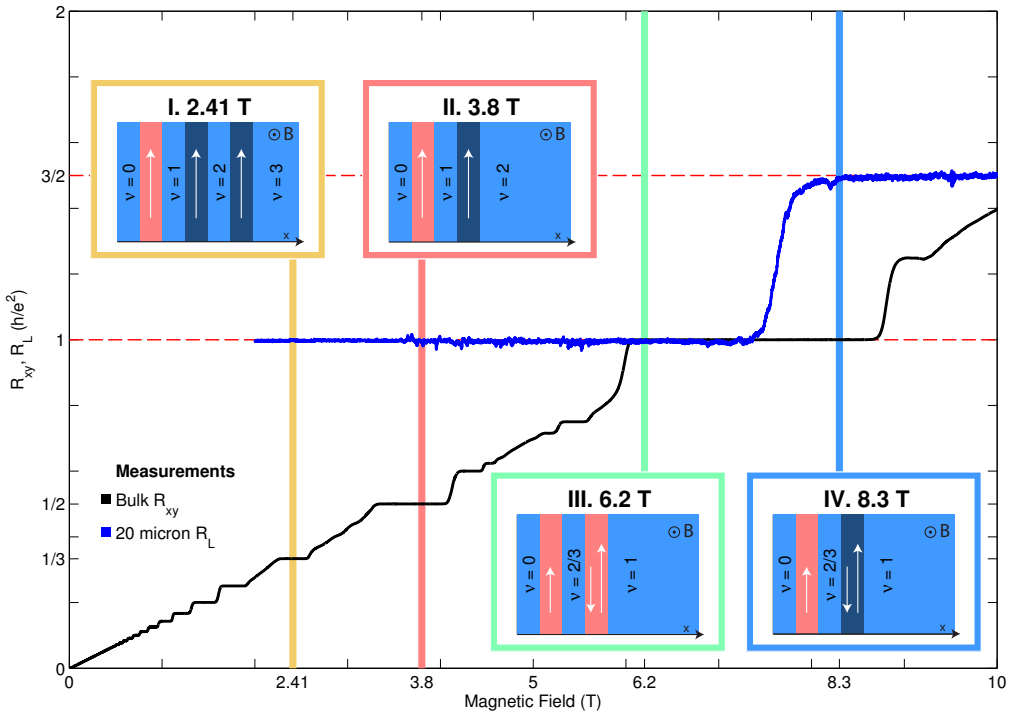

Figure 2: Magnetic field dependence of the Hall resistance R_{xy} (black), and the local Hall resistance R_L (blue). The local Hall resistance is measured using the central QPC as a current source (~ 10 pA) and a downstream QPC as a voltage probe. Plateaus in R_L reveal the structure of the edge, and also indicate which edge channels participate in charge transport. The insets depict the qualitative structure of the sample edge at various magnetic fields, with incompressible regions shown in light blue and labeled by filling factor. In the intervening compressible channels, arrows point in the direction of charge flow, while the arrow length specifies a charge conductance of $G = 1$ or $G = 2/3$ in units of e^2/h. The channels highlighted in red contribute to charge transport at the voltage probe. I,II) When the bulk filling factor is $\nu = 2$ or $\nu = 3$, the edge is composed of integer channels with the outermost channel having conductance $G = 1$. At the voltage probe, the excess current is carried solely by the outermost channel. III,IV) Outside the bulk $\nu = 1$ state the edge is reconstructed, resulting in an outermost $G = 2/3$ charge channel. The remaining $1/3$ conductance can be found on a spatially separated inner edge located in the compressible region between the $\nu = 2/3$ and $\nu = 1$ incompressible regions. At 8.3 T, the excess current is carried to the voltage probe only by the outermost channel. At 6.2 T, the edge channels come to the same potential before reaching the voltage probe, resulting in $R_L = 1$.

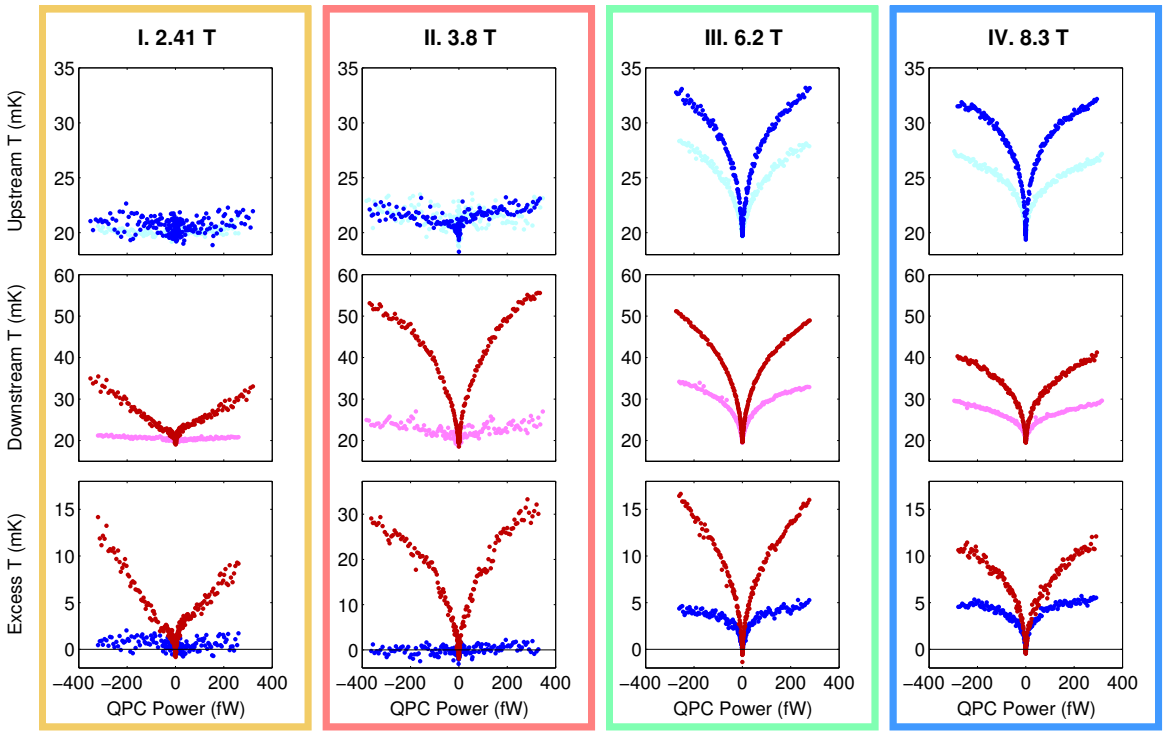

Figure 3: Dependence of the local edge temperature on the power dissipated in the QPC ($|I|\cdot\Delta V_{QPC}$), at different magnetic fields. Negative (positive) QPC powers correspond to the injection of holes (electrons). For each magnetic field, the upstream and downstream temperatures were measured with (blue, red) and without (cyan, magenta) the deflector gates energized. With the deflectors at zero voltage the edge channels are directed to floating ohmic contacts where equilibration occurs. The difference between temperatures with and without the deflectors energized, for the same dot, yields the local change in temperature due to the heat carried by the edge. This excess temperature for the downstream (red) and upstream (blue) dots is plotted across the bottom row, for each magnetic field. For I and II, corresponding to an integer outermost edge, heat is carried chirally downstream with no upstream heat transport. For IV, where we measure a 2/3 outermost edge, the heat is carried downstream and upstream. For III, heat is also carried in both directions, while $R_L = 1$. We attribute this behavior to reconstruction outside the bulk $\nu = 1$ edge, which allows upstream heat transport without 2/3 charge transport.

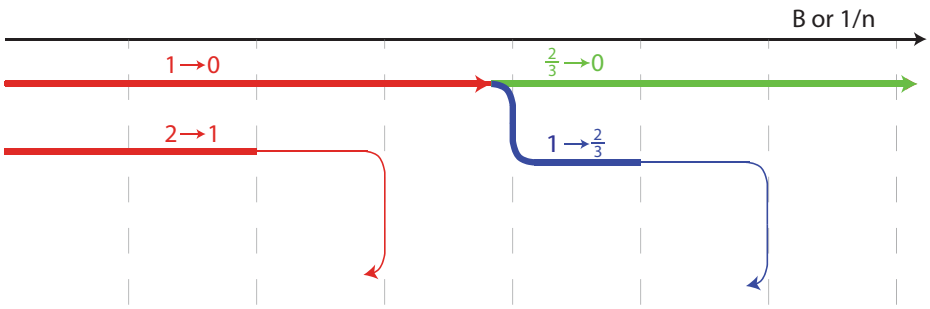

	(I)	(II)	(III)	(IV)	(V)	(VI)
R_{xy}^{-1}	2	2	1	1	1	2/3
R_{L}^{-1}	2	1	1	1	2/3	2/3
upstream heat	no	no	no	yes	yes	yes

Figure 4: One possible evolution of edge structure as a function of magnetic field. Three types of edges are present in this experiment, denoted by different colors, with the topmost edge being the outer edge. Only edge structures II, IV, and V are present in the device in Fig. 1. Edge III is presented in an online supplement. All resistances are given in units of $\frac{h}{e^2}$. A measurement of R_{xy} allows one to determine the total conductance of all edges. A measurement of R_L allows one to determine which edges chemically equilibrate when charge is injected into the outer edge (denoted by bold lines in the figure). Only the $\frac{2}{3} \rightarrow 0$ edge transports heat upstream, and can be identified by our thermometry measurements. Detecting upstream heat allows us to discriminate between edges III and IV (see SOM D).

Supplement A: Chemical Potential Measurements and Thermometry

I. Chemical Potential Measurement

As the DC current I injected through the QPC increases, the downstream chemical potential of the outermost edge component must correspondingly rise. Unless a DC voltage bias V_{ZB} is applied to O5 to exactly compensate this altered chemical potential, a DC current will flow through the dot whenever the Coulomb blockade is lifted. Tuning the dot to this zero bias condition allows us to measure the chemical potential of the outermost edge component. In principle an upstream charge current may cause a similar rise in chemical potential at the upstream dot. For all measurements, the upstream chemical potential was indistinguishable from that of the ground contact (O7), suggesting that upstream charge transport does not occur on a 20 μm scale.

The dependence of V_{ZB} on the current I, at a particular value of magnetic field, measures the total conductance of the edge channels participating in charge transport at the quantum dot. For the deflector gates energized, this conductance matches $1/R_L$. When the deflector gates are at zero voltage, however, all edges carry charge and the total conductance matches the Hall conductance. These observations corroborate the assertion that the deflector gates are able to direct the flow of edge channels. When the deflector gates are energized, the data also show that charge remains in the outermost edge on a 20 μm scale even during thermometry measurements. An example of edge resistances determined using the quantum dot zero bias condition is presented in Figure S1.

II. Coulomb Blockade Thermometry

At each value of the magnetic field, quantum dots were tuned to the Coulomb blockade (CB) regime. The typical charging energy was 50 μeV, while the typical spacing between CB peaks corresponded to 20 mV on the plunger gate. We calibrated each dot individually for thermometry measurements by extracting the slopes m_1 and m_2 of CB diamonds adjacent to the conductance peak of interest, as shown in Figure S2. The lever arm $\alpha = C_G/C$ was then determined by

$$\alpha = \frac{|m_1 m_2|}{|m_1| + |m_2|}, \tag{1}$$

where C_G is the capacitance between the dot and the plunger gate, and C is the total capacitance. Knowing α allows the use of the conductance peak width as a sensitive thermometer. Our dots are in the metallic regime $\triangle E \ll k_B T \ll e^2/C$, where the temperature far exceeds the dot level spacing $\triangle E$. The temperature of the leads is then found through the formula for the lineshape of a conductance peak centered at gate voltage V_R :

$$G \propto \cosh^{-2}\left(\frac{e \cdot \alpha \cdot |V_R - V_G|}{2.5 k_B T}\right). \tag{2}$$

During the experiment, we applied a fixed 4 μV AC voltage bias and a variable DC voltage bias to each dot (contacts O1 and O5 in Figure 1). The different AC frequencies used for each dot were typically 215 and 315 Hz. To determine the temperature T of the leads coupled to a single dot, we first tuned the DC voltage bias V_{DC} applied to the dot so that the chemical potentials of the two leads were equal, as described above. Then the plunger gate voltage V_G was swept through a conductance peak while the resulting AC current was monitored using lockin techniques. The typical AC dot resistance was > 100 kΩ, resulting in AC currents of ~ 10 pA. For each DC current I injected through the QPC, the temperature of the leads was extracted using equation (2). Representative scans over conductance peaks in the downstream dot, for two different injected currents, are plotted in Figure S3.

A data set consisted of one sweep of the DC voltage bias V_{bias} applied to the QPC (contact O3), between -250 μV and 250 μV. At each value of V_{bias} we recorded the injected current I, as well as the temperature T and chemical potential μ for both dots. The QPC power was defined as the vector $P_{QPC} = I \cdot V_{bias} - I^2(h/\nu e^2)$, where ν was the bulk filling factor. For each sweep, the electron temperatures found using equation (2) were normalized such that the minimum electron temperature was

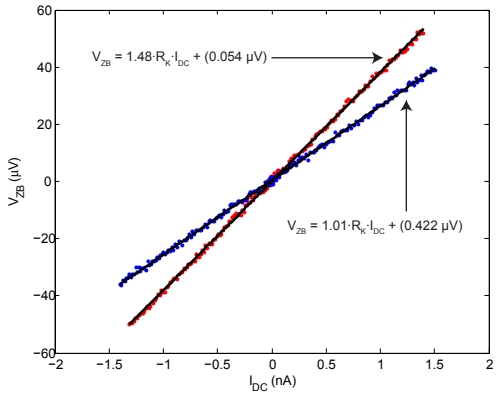

Figure S1: The voltage V_{ZB} applied to O5 in order to zero the bias across the downstream quantum dot, as a function of the current I_{DC} injected through the QPC. Data were acquired at a magnetic field of 8.3 T. For the deflector gates energized, V_{ZB} is shown in red, with a slope corresponding to current carried by a $\nu = 2/3$ outermost edge. When the deflector gates are set to zero, V_{ZB} is shown in blue, indicating conduction of current by edges with total conductance $G = 1$.

always 20 mK, equivalent to an effective rescaling of α. This minimum electron temperature of 20 mK was measured at the base temperature of our dilution refrigerator via Coulomb blockade thermometry, for quantum dots with cold leads sourced directly from ohmic contacts. We assume in our experiment that all edges are at this minimum temperature when $V_{bias} = 0$. For a dot coupled to a fractional edge, electronic correlations may alter the temperature extracted using equation (2). As long as the peak width remains linear in temperature as a result of such behavior, our procedure accurately reports relative edge temperatures. The absolute fractional edge temperatures may then differ from our reported data by an overall normalization.

While all of our reported Coulomb blockade temperatures use the above rescaling to normalize the base temperature to 20 mK, it is also possible to calibrate temperatures using the resistive RuO thermometer on the mixing chamber. In Figure S4 such a calibration is plotted, showing how the temperature deduced from Coulomb blockade peaks corresponds to the mixing chamber temperature. The behavior is linear at high temperatures and saturates to the minimum dot temperature of 20 mK at low temperatures due to the decoupling of the electronic system from the lattice. Because the mixing chamber thermometer is not directly coupled to the two-dimensional electronic system, we have chosen to normalize minimum temperatures to 20 mK rather than calibrate using the mixing chamber. From this data we see that a calibration using the mixing chamber thermometer does not significantly alter our results beyond a ~140% temperature rescaling at the highest reported temperatures. None of our qualitative claims are changed by such a rescaling, and this temperature increase cannot explain the temperature deficiency discussed in the main text and Supplement B.

We accumulated several normalized data sets at each value of magnetic field, both with the deflector gates energized and at zero voltage. To determine the increase in temperature at the downstream dot due to heat carried by the outermost edge component, we first separated the data sets into two groups, depending on whether the deflectors were energized or at zero voltage while the data was taken. For each group, the normalized downstream temperatures were then averaged to obtain two vectors containing the mean downstream temperatures for both deflector settings. The QPC powers were similarly averaged, resulting in the power-dependent mean temperatures plotted in Figure 3. The difference between the mean downstream temperatures, for equal QPC power, was reported as the excess downstream dot temperature. This procedure was also used for the upstream dot, and for all reported values of the magnetic field. The excess temperatures determined in this way are plotted in the third row of Figure 3 of the main paper.

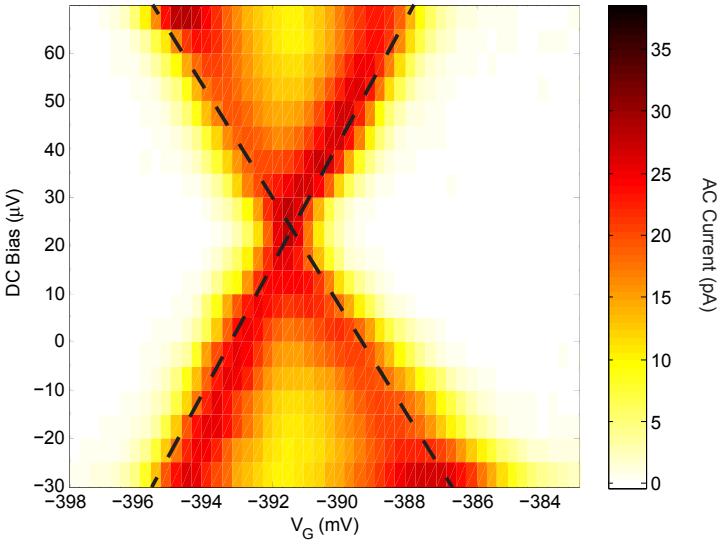

Figure S2: Coulomb blockade data used to calibrate the downstream quantum dot at a magnetic field of 8.3 T. The lever arm α is calculated from the slopes of the zero-conductance regions, marked by dashed lines.

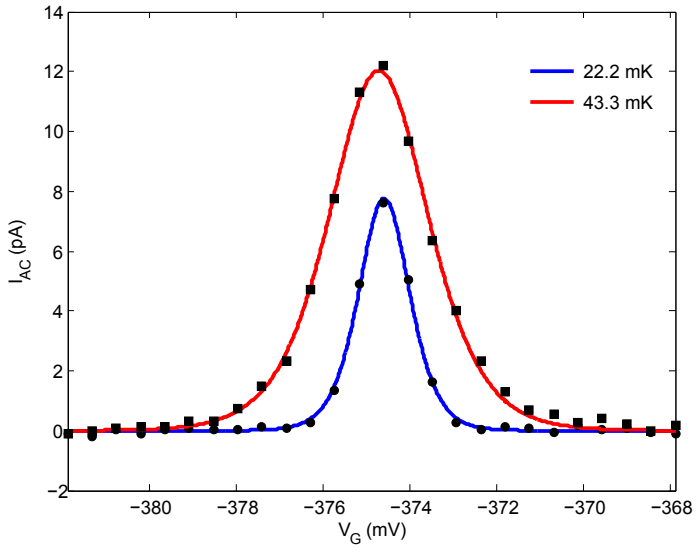

Figure S3: AC current I_{AC} through the downstream quantum dot as a function of the plunger gate voltage V_G, measured at a magnetic field of 8.3 T. Black circles (squares) correspond to data taken for an injected QPC current $I = 0$ nA ($I = 1.5$ nA). The best fits of the data to equation (2) are shown in blue and red, and give temperatures of $T = 22.2$ mK for $I = 0$ nA and 43.3 mK for $I = 1.5$ nA.

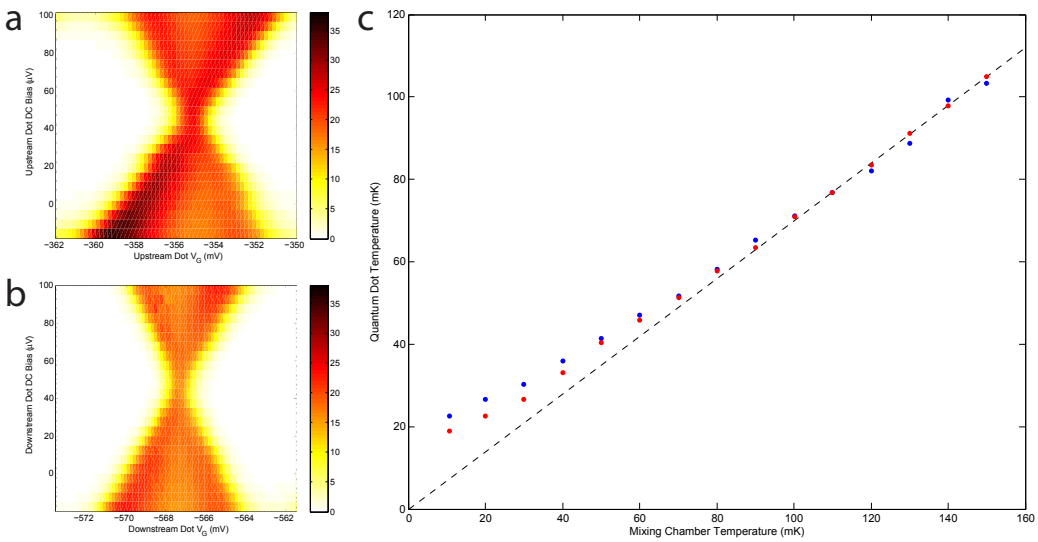

Figure S4: Comparison of Mixing Chamber and Coulomb Blockade Thermometry, at 6.15 T. Heat is applied to the mixing chamber and temperatures are measured using a resistive RuO thermometer attached to the mixing chamber along with the two patterned quantum dots. a,b) Widths for the CB thermometers are calibrated using the diamonds. c) The widths of our CB peaks are linear in temperature, except for a saturation at 20 mK as the mixing chamber is cooled to 10 mK.

Supplement B: Power carried by Non-Equilibrium Edges

In our experiment, we tune the bulk quantum Hall state to filling factor ν, and apply a voltage V between ohmic contacts O3 and O6. These two contacts are separated by a QPC tuned to have resistance $R \sim 100$ kΩ. When a net current I is injected through the QPC, the electronic occupation of the outermost compressible edge channel deviates locally from its equilibrium distribution. Quantum dots placed 20 μm upstream and downstream of the QPC probe the chemical potential and temperature of this outermost edge. The form of Coulomb blockade peaks monitored during our heat transport measurements suggests that the outer edge internally reaches thermal equilibrium over a distance smaller than 20 μm. However, our charge measurements indicate that chemical equilibration of the outer edge with inner edge channels starts to occur at a distance greater than 20 μm. Thus, at the downstream measurement point the outermost edge has a Fermi occupation function and carries all of the injected current I. For the measurements at magnetic fields of 2.41 T and 3.8 T (bulk $\nu = 3$ and $\nu = 2$), the electrical conductance of this edge is consistent with downstream charge transport by a single integer quantum Hall (IQH) edge. Furthermore, our thermometry measurements show strict downstream heat transport, also consistent with the IQH regime. To determine the expected quantitative outcome of our measurements in the IQH regime, we analyze charge and heat transport by IQH edges in the experimental system described above.

The chemical potential μ of an IQH edge is related to the current I_E that it carries:

$$I_E = \frac{e}{h}\mu. \tag{3}$$

In our model, the total number of edge channels on each side of the QPC is equal to the bulk filling ν. However, since only the outermost channel contributes to charge transport on a 20 μm scale, we treat inner channels as inert and consider only the behavior of the outer channel. The two outer edges that carry charge toward the QPC originate in ohmic contacts O3 and O6. The occupations of these incoming edges are therefore Fermi functions,

$$\begin{aligned} f_{in}^{O3}(E) &= f(E - \mu_{in}^{O3}, T_{base}) \\ f_{in}^{O6}(E) &= f(E - \mu_{in}^{O6}, T_{base}), \end{aligned} \tag{4}$$

where $\mu_{in}^{O3} = \mu + eV$ and $\mu_{in}^{O6} = \mu$ are the chemical potentials of O3 and O6 and $T_{base} = 20$ mK is the electron base temperature. At the QPC, the electronic occupations of the outgoing edge modes are forced out of equilibrium. At a distance 20 μm from the QPC these outgoing edges reach thermal equilibrium, with chemical potentials $\mu_{out}^{O3} = \mu + eV - (h/e)I$ and $\mu_{out}^{O6} = \mu + (h/e)I$ determined using equation (3). While these chemical potentials can be found simply by considering charge transport, a more detailed analysis of scattering at the QPC is necessary to determine the temperatures of the outgoing edges.

The equilibrium temperature T of an IQH edge is related to the power J_E carried by its excitations according to

$$J_E = \frac{(\pi k_B)^2}{6h} T^2. \tag{5}$$

In general J_E can also be calculated from the occupation $n(E)$ and chemical potential μ of an edge, by integrating the power:

$$J_E = \frac{1}{h}\int_0^{\mu} dE \cdot (\mu - E) \cdot (1 - n(E)) + \frac{1}{h}\int_{\mu}^{\infty} dE \cdot (E - \mu) \cdot n(E). \tag{6}$$

Here the first integral corresponds to the contribution of hole-like excitations, while the second integral corresponds to particle-like excitations. The 1D relation $g(E) \cdot v(E) = 1/h$ between the velocity $v(E)$ and density of states $g(E)$ was used to simplify the integrals.

Since the outgoing edges in our model have non-equilibrium distributions $n_{out}^{O3}(E)$ and $n_{out}^{O6}(E)$ immediately after the injection of current I, their respective energy currents are determined using equation (6). At a distance 20 μm from the QPC, the outgoing edges are in equilibrium. If no energy

escapes from the edge as it equilibrates, equation (5) then provides a calculation of the expected edge temperatures. With the goal of ultimately finding these temperatures, we therefore consider the forms of the non-equilibrium edge distributions, which depend on the energy-dependent QPC transmission probability $\tau(E)$. This transmission is determined by the differential conductance dI/dV of the QPC, as follows:

$$I = \int_0^\infty dE \cdot \tau(E) \cdot (f_{in}^{O3}(E) - f_{in}^{O6}(E)). \tag{7}$$

Using τ and the distributions of the incoming edges (4), we find expressions for the non-equilibrium distributions:

$$\begin{aligned} n_{out}^{O3} &= (1-\tau) \cdot f_{in}^{O3} + \tau \cdot f_{in}^{O6} \\ n_{out}^{O6} &= (1-\tau) \cdot f_{in}^{O6} + \tau \cdot f_{in}^{O3}. \end{aligned} \tag{8}$$

From these distributions we can then deduce the partitioning of power among the outgoing edges, as well as the outgoing equilibrium temperatures T_{out}^{O3} and T_{out}^{O6}. We find that each outgoing edge carries an equal energy current. Conservation of energy provides a constraint on the total outgoing power:

$$I \cdot V - I^2(h/e^2) = \frac{(\pi k_B T_{out}^{O3})^2}{6h} + \frac{(\pi k_B T_{out}^{O6})^2}{6h} - \frac{(\pi k_B T_{base})^2}{3h}. \tag{9}$$

This relationship holds as long as the inner edges remain decoupled from the outermost edge modes. Here the left-hand side specifies the power dissipated by the QPC, while the right-hand side represents the net power carried away by edge excitations. The term $I^2(h/e^2)$ refers to energy dissipated at ohmic contacts, and does not contribute to heating the edge. For completeness, the distributions of the outgoing edges, 20 μm from the QPC, are given below:

$$\begin{aligned} f_{out}^{O3}(E) &= f(E - \mu_{out}^{O3}, T_{out}^{O3}) \\ f_{out}^{O6}(E) &= f(E - \mu_{out}^{O6}, T_{out}^{O6}), \end{aligned} \tag{10}$$

In Figure S5, numerical calculations of the outermost edge occupation functions are plotted during each stage of scattering at the QPC, for an applied voltage $V = 175$ μV and at bulk filling $\nu = 2$. In panel B, the incoming distributions are shown with the QPC transmission τ extracted from IV data. In panels C and D, the non-equilibrium and equilibrium distributions are plotted for outgoing edges on each side of the QPC. For the equilibrium outgoing distributions, we extract the temperatures T_{out}^{O3} and T_{out}^{O6} over a range of V to determine the dependence of edge temperatures on the QPC power $P_{QPC} = I \cdot V - I^2(h/e^2)$. As shown in Figure S6, our model qualitatively explains the cusp in temperature that is observed at $P_{QPC} = 0$.

Using this model, we expect the downstream quantum dot to measure a maximum temperature of 560 mK for $\nu = 2$ and 545 mK for $\nu = 3$. The actual observed maximum temperatures were 55 mK for $\nu = 2$ and 35 mK for $\nu = 3$. Although we observe no charge leakage to inner edge channels on a 20 μm scale, the loss of heat to inner edges is still possible and would decrease the expected temperatures. If all edges equilibrate thermally over a distance smaller than 20 μm, we expect that the power J_E carried by the outermost edge will be divided by the filling factor ν. Using equation (5), it follows that the temperature will be divided by $\nu^{1/2}$. For this type of thermal equilibration we thus expect to measure 395 mK for $\nu = 2$ and 315 mK for $\nu = 3$. Whether or not heat escapes to the inner edges, it is still clear from this analysis that in our experiment the majority of the power dissipated in the QPC does not find its way to the outermost edge.

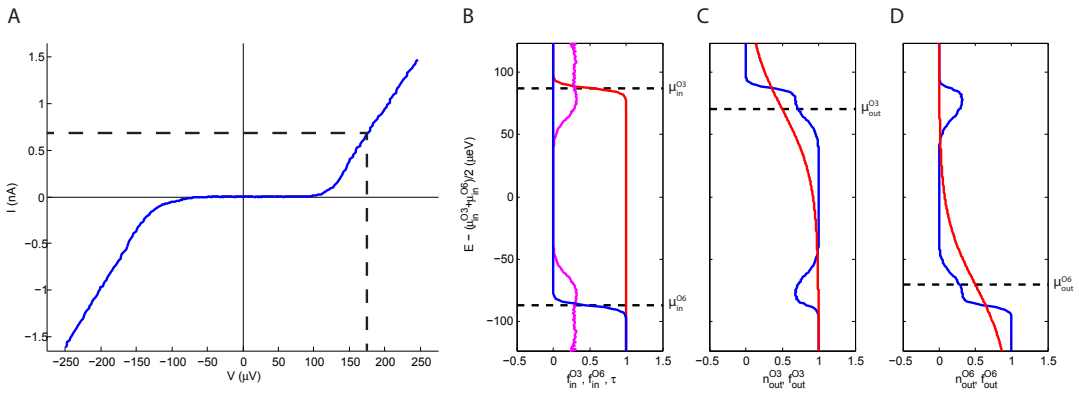

Figure S5: A) The IV curve of the QPC at bulk filling $\nu = 2$. An applied voltage $V = 175$ μV was used to calculate the distributions shown in (B-D). This voltage and the corresponding injected current are marked with dashed lines. B) The QPC transmission probability τ, calculated from the QPC IV curve, is shown in magenta. In blue (red), the occupation f_{in}^{O6} (f_{in}^{O3}) of the incoming outer edge mode originating at ohmic contact O6 (O3). The chemical potentials differ by $eV = 175$ μeV. C) In blue, the non-equilibrium occupation n_{out}^{O3} of the outermost edge immediately after the injection of current through the QPC. This edge component carries charge toward O3. 20 μm from the QPC, the edge is in equilibrium with the distribution f_{out}^{O3}, shown in red. C) The edge component carrying charge toward O6 has the non-equilibrium occupation n_{out}^{O6}, shown in blue, immediately after current is injected. 20 μm downstream the edge has equilibrated to the distribution f_{out}^{O6}, shown in red.

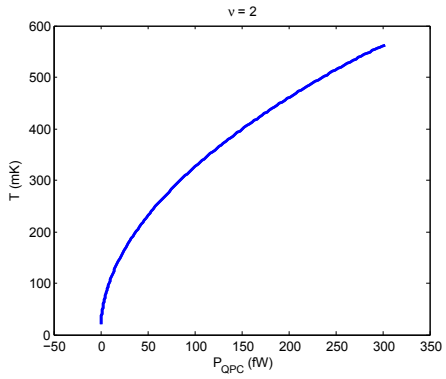

Figure S6: Expected equilibrium temperatures of the outgoing outermost edges, calculated using the measured QPC transmission τ at $\nu = 2$. Both outgoing edges are expected to have the same temperature. The $\nu = 3$ data give the same temperature as a function of QPC power.

Supplement C: Bulk Heat Transport

As mentioned in the main text and Supplement B, we observe temperatures well below what is expected for a system of quantum Hall edges with no energy dissipation. This necessarily means that heat diffuses out of the edges into additional modes in either the bulk of the 2D electronic system or the surrounding crystalline solid. Because we see a bulk contribution to heating when the bulk is at $\nu = 1$ (Columns III and IV of Figure 3), but not when the bulk is at $\nu = 2$ or $\nu = 3$ (Columns I and II), and because we don't expect a change of magnetic field to significantly affect heat conduction through the solid, we can attribute the heating at high fields to the $\nu = 1$ electronic system. While we don't know the mechanism of this bulk heat transport in such a strongly insulating state, we suspect it may be associated with low energy spin degrees of freedom that exist at $\nu = 1$.

The presence of this bulk heat transport in the two measurements where we see upstream heat transport attributed to edges requires some additional discussion.[1] Specifically, we need to rule out the possibility that turning our deflectors on and off affects the quantity of heat transported by the bulk to the thermometers, thereby producing a signal unrelated to edge heat transport. Below we describe two experiments specifically designed to address this possibility. Our findings provide two important observations. Firstly, our gates are not completely effective at preventing the flow of heat. We inferred this from the shape of our Coulomb blockade peaks, and checked it explicitly by attempting to block heat flow with a gate. Secondly, if we reduce the length of the deflector gates to the point where there is much less bulk $\nu = 1$ region for heat to diffuse upwards into when the deflectors are off, we observe the same qualitative and quantitative behavior that was presented in the main body of the paper. Both of these observations are discussed more carefully below.

I. Diffusion of heat through gated regions

When our topgates are energized to completely deplete carriers from the underlying 2D electron system, we would expect that energy can no longer be transported by that system. However, heat that manages to diffuse into the lattice can still propagate. Here we will present data suggesting that some heat does indeed diffuse across the depleted regions.

The first indication of such diffusion is taking place can be seen in the form of our Coulomb blockade peaks. The fits we used in the experiment assume that the temperatures of the two quantum dot leads are identical. However, since we are only explicitly heating one side of the dot, a simple model suggests that we should expect leads with different temperatures. This temperature asymmetry should show up as an increased kurtosis in the CB peak shape. In Figure S7, we show the one-temperature fit that was used in the main body of this paper along with two alternatives that allow for asymmetric lead temperatures. This particular peak corresponds to the downstream measurement at a magnetic field of 6.2 T and an injected power of 274 fW. The deflector gates are energized, so this peak includes both edge and bulk contributions.

Figure S7b presents an alternative fit with an additional fit parameter that allows for different temperatures in the two leads. While the one-temperature fit suggests lead temperatures of 51 mK, the two temperature fit suggests that one of the leads is hotter (60 mK) and the other is colder (39 mK). However, even though the fits are consistently better with the extra parameter, the residuals are not systematically cleaner. Figure S8 presents a comparison of the one-temperature and two-temperature fits for the entire range of injected powers that we studied. Below 50 fW of injected power, the one-temperature and two-temperature fits agree exactly, suggesting equal temperature leads. At higher powers, the two temperature fit does suggest a difference in the lead temperatures. Even this asymmetry, however, has to be considered carefully. Because there are nearby peaks (roughly 800 mK away from the peak center, when translated from gate voltage as in Figure S7), at high temperatures we can expect them to artificially distort our peak and increase the quality of an asymmetric-temperature fit.

Figure S7c presents yet another fit which assumes that the cold lead has the naively expected temperature of 20 mK, corresponding to the observed base temperature for electrons with no intentional

[1] A measurement where bulk heat transport is present without edge heating is presented in Supplement D

heating. The temperature of the hot lead is allowed to vary. With this constraint, the best fit suggests a hot lead temperature of 59 mK. Here, however, the residuals have a pronounced trend that persists for all fits with the 20 mK constraint.

Without strong evidence that a two-temperature fit better describes our measurements, we opted to use a single-temperature fit for the main data presented. None of the qualitative observations of bulk heat transport or upstream heat transport by a neutral edge mode are affected by using the hotter temperature from two-temperature fits. Furthermore, the two-temperature fit doesn't solve the temperature deficiency alluded to in the main text or Supplement B.

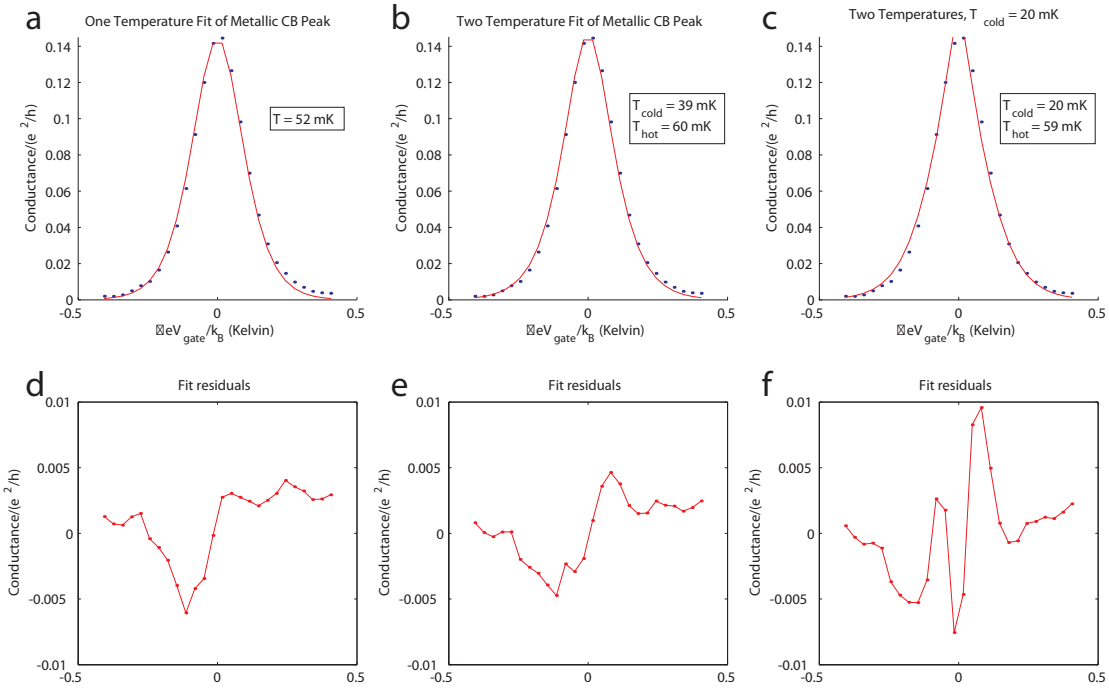

Figure S7: **a)** One temperature fit of the CB peak seen downstream at 6.2T and 274 mW of injected power. The deflector gates are energized, so this peak includes both edge and bulk contributions. Additional peaks are centered roughly 800 mK to the left and right of the center of this peak. **b)** Fit obtained by adding an additional parameter allowing for asymmetric lead temperatures. There is no systematic improvement in the residual trend by using such a fit (though the quality of fit obviously improves slightly). **c)** Fit obtained using the same form as panel b, but fixing the cold lead to a 20 mK distribution. This produces a low quality of fit and certainly doesn't describe our data well. **d,e,f)** Fit residuals plotted below the associated fit

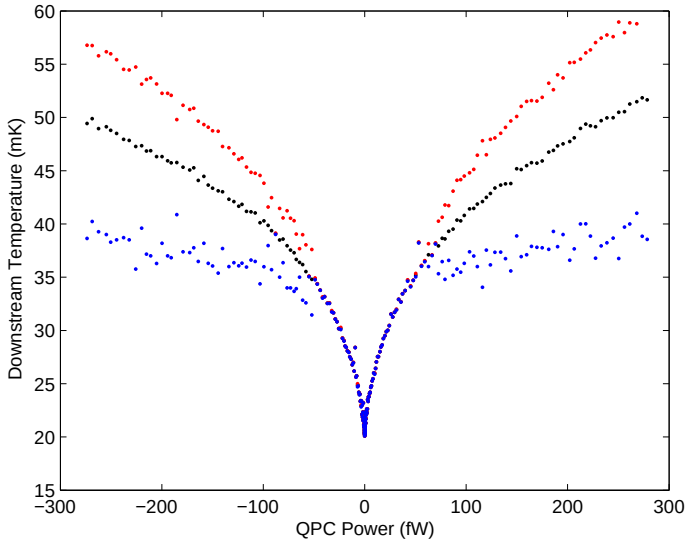

Figure S8: Temperature fit of the CB peak seen downstream at 6.2T as a function of injected power. Black denotes the one-temperature fit (as in Figure S7a), and red and blue denote the hot and cold temperatures of a two-temperature fit (as in Figure S7b). They agree perfectly at low injected powers, but begin to diverge beyond 50 fW.

We can go further and explicitly test for heat transport across depleted regions by placing a strip of such a region between our heater and our thermometers, as in the device pictured in Figure S9. Any heat detected at the thermometers would necessarily have to diffuse through depleted region beneath the vertical gates. Results of this test are depicted in Figure S10. Here, we can clearly see that some heat flows through these narrow depleted regions. At the highest injected power, we see the temperature rise from 20 mK to 28 mK with an uninterrupted 2D and a temperature rise to 22 mK with the 2D depleted beneath the vertical gates. This small heat diffusion through gated regions is qualitatively consistent with our observation of heating in the cold leads of our quantum dots, as mentioned above. The fact that the temperature is reduced from the ungated value (22 mK versus 28 mK) provides additional evidence that the 2D electron system is responsible for the observed bulk heat transport at high fields.

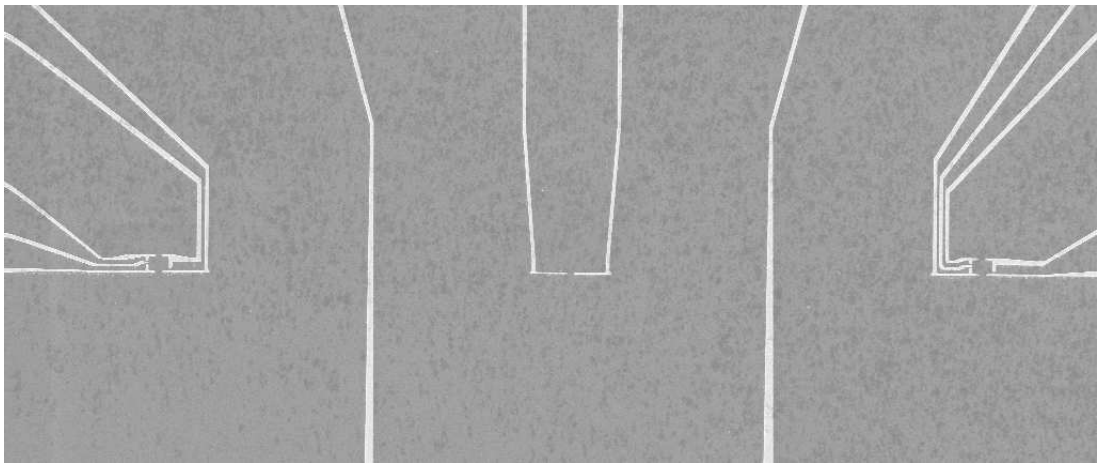

Figure S9: Device designed to explicitly test for heat leakage across a depleted barrier. When the vertical gates are energized, the 2D systems on the left and right are completely isolated (electrically) from the 2D system with the heater in the center.

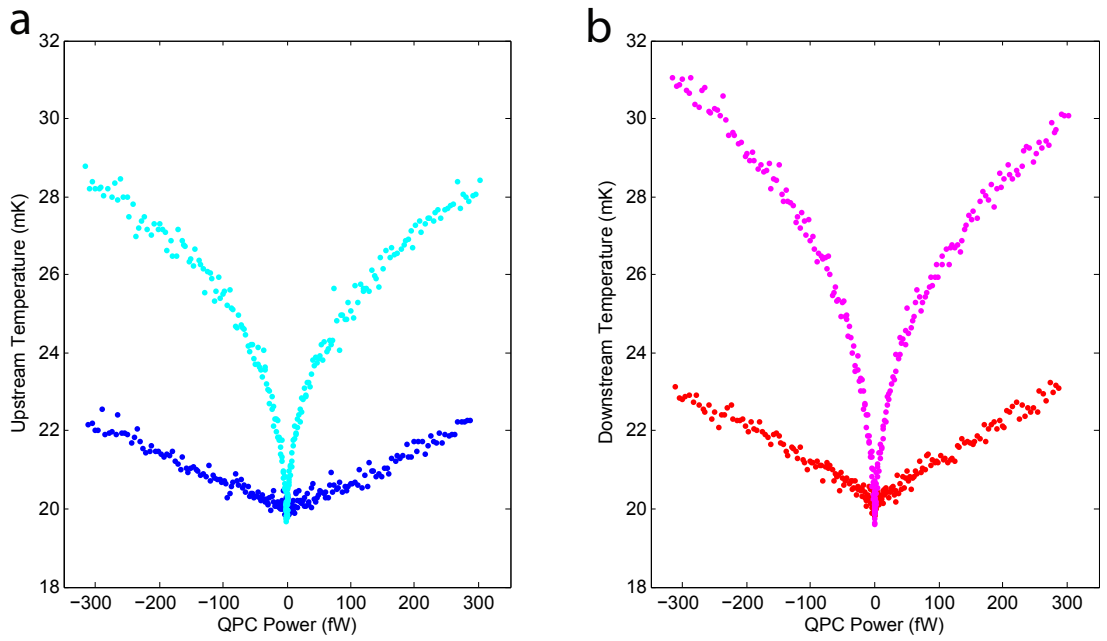

Figure S10: Heat transport across a depleted barrier. The cyan curve depicts temperature measured upstream from the heater when the vertical gates are deenergized. The blue curve depicts the temperature when the vertical gate is energized, so heat must diffuse across a depleted region. The magenta and red curves are the corresponding traces for the downstream dot. All data was taken at 8.3 T, corresponding to column IV in Figure 3 of the main paper.

II. Geometric Diffusion Considerations

Because we only detect neutral mode heating when there is a bulk contribution to the heating signal, we have to ensure that there is no significant change in the bulk contribution as we energize and deenergize the deflector gate. It would appear plausible, for instance, that by turning on the deflector gate we reduce the area over which the bulk heat can diffuse. Specifically, with the deflector gate on, heat can no longer diffuse up into the 2D region between our heater and our thermometers. As a result, one may conjecture that more heat will be directed towards the thermometers resulting in a higher temperature unassociated with quantum Hall edge physics. The first indication that this redirection of heat isn't relevant is the above observation (from CB peak shapes and direct measurements) that heat does indeed partially diffuse through depleted regions. A more convincing test, however, consists of altering the geometry of the bulk to reduce the effect of this geometric distortion.

To this end, consider the device shown in Figure S11b. It is identical to the devices used for measurements in the main body of the paper, but with a shorter deflector gate length (8 um instead of 15 um). At 8.3 T, we expect an edge structure as shown in Figure S11, with two separated edges: one corresponding to the boundary between vacuum and $\nu = \frac{2}{3}$ and the other corresponding to the boundary between $\nu = \frac{2}{3}$ and $\nu = 1$, as $\nu = 1$ is the bulk filling factor and $\nu = \frac{2}{3}$ is the edge that we detect with our local injection measurements. In the 8 um deflector device, with the deflector deenergized, we measure a slightly elevated resistance ($1.19\,R_K$), indicating that the inner edge corresponding to the transition from $\nu = \frac{2}{3}$ to $\nu = 1$ is being backscattered (transmission coefficient of 52% for that inner edge). This indicates that the $\nu = 1$ bulk is largely closed off in this deflected region, so we would expect very little bulk heat to diffuse upwards through this narrow constriction. If the difference in upstream heating displayed in Figure 3(IV) of the main paper is due to a redirection of bulk heat flow, we would expect almost the same difference between the temperature measured in the 15 um deflector device (Figure S11a) and the 8 um deflector device (Figure S11b).

The data from these measurements are presented in Figure 12. The blue and red points correspond to temperatures measured in the device from Figure S11a with deflectors off. The cyan and magenta points correspond to temperatures measured in the device from Figure S11b, also with deflectors off. These undeflected temperatures in the two devices are very close, to within the data spread. For reference, the temperature associated with turning on the deflectors (which results in the same geometry for the two devices) is displayed in green and orange.

From these, we can infer that the excess temperature found in the green and orange traces is indeed associated with a hot $\nu = \frac{2}{3}$ edge, as this edge is the only component of the system that is significantly altered as deflector gates are turned on in the device from Figure S11b.

In SOM D, we present yet another device, where the gate-defined edge is replaced by a sharp mesa-defined edge. If the excess upstream heat was due to a redirection of bulk heating, we would expect an elevated temperature in that situation, given that the device possesses a nearly identical bulk geometry to the gate-defined system. Here, however, we don't see any heat associated with the edge at 6.2 T (Fig. S14a). This provides even further evidence that the observed upstream heat is due to FQH edge structure and is independent of the measured bulk heat transport at $\nu = 1$.

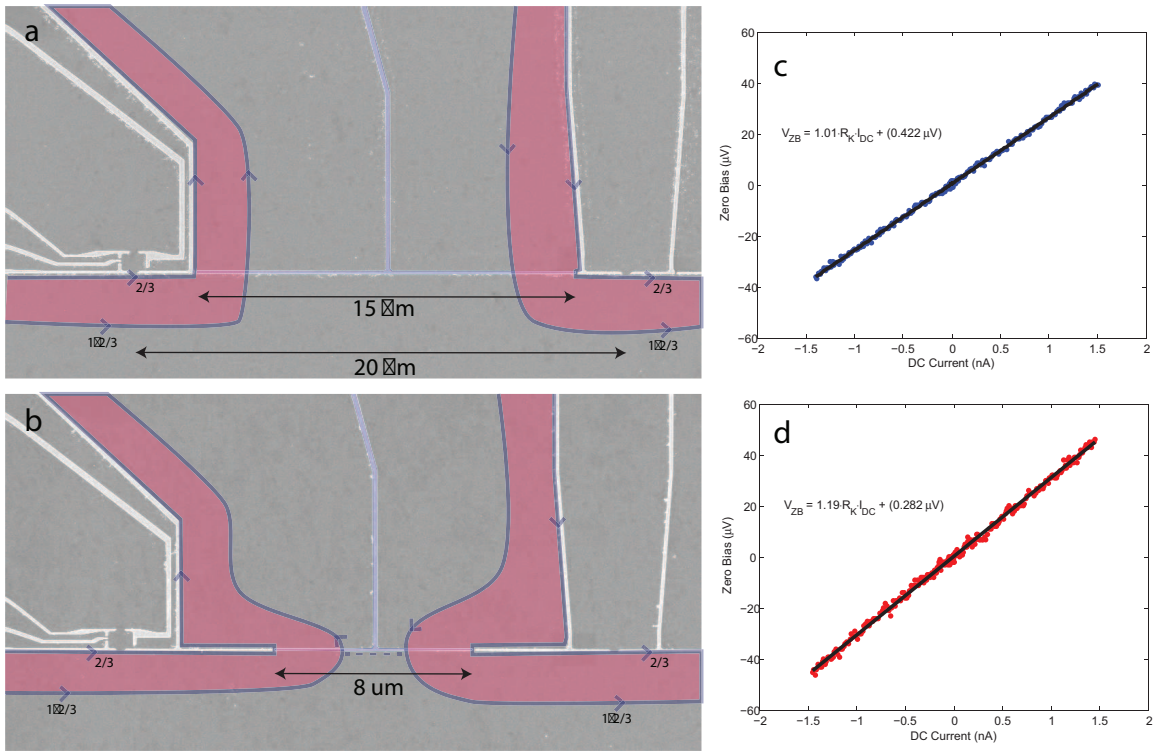

Figure S11: A device to test the effect of geometric diffusion considerations. **a)** SEM image of device identical to that used for data in the main paper. Edge labels correspond to what is expected at a field of 8.3T, based on our local and global R_{xy} measurements. **b)** SEM image of a device with a narrower region through which edges can be deflected. From the elevated resistance shown in panel d, we know that the inner edge is partially backscattered. **c)** Copy of the ΔV_{ZB} versus I_{DC} curve from Figure S1, demonstrating that the resistance in the deflector channel is the same as the bulk value ($1.01R_K$), indicating that the $\nu = 1$ state is fully connected from the top to the bottom of the image in panel a. **d)** A corresponding ΔV_{ZB} versus I_{DC} curve for the device in panel b. The elevated resistance ($1.19R_K$) indicates that the inner edge, which has a conductance of $\frac{e^2}{3h}$ is 52% transmitted. This suggests that the $\nu = 1$ state is connected through a narrow channel in this device, providing much less room for heat to diffuse upwards compared to the device in panel a

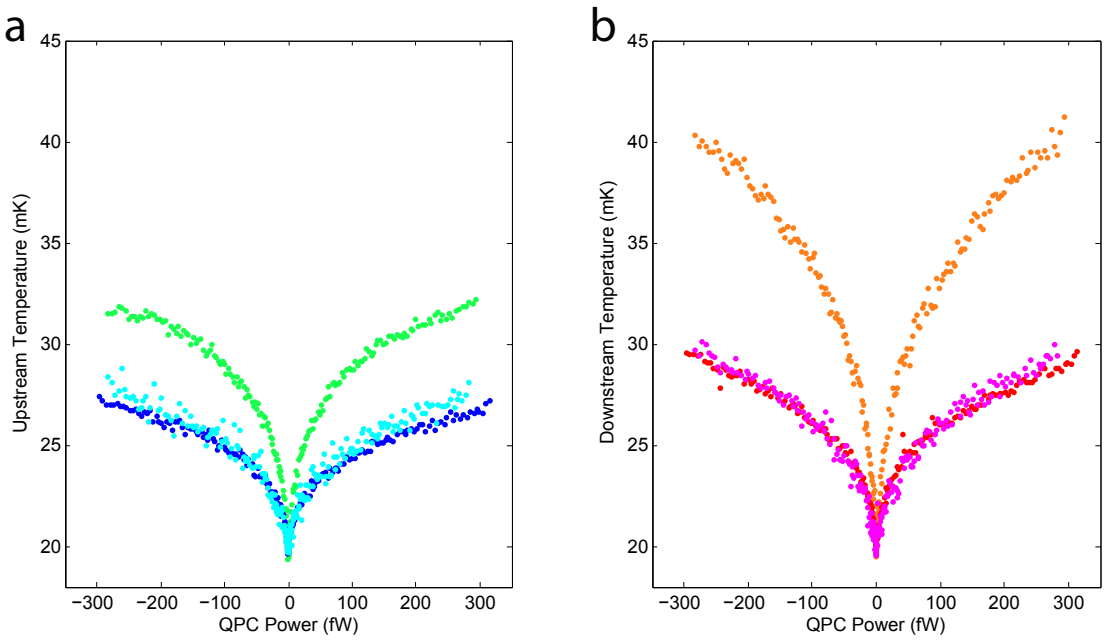

Figure S12: The blue and red points correspond to temperatures measured in the device from Figure S11a with deflectors off. The cyan and magenta points correspond to temperatures measured in the device from Figure S11b, also with deflectors off. These undeflected temperatures in the two devices are very close, to within the data spread. For reference, the temperature associated with turning on the deflectors (which results in the same geometry for the two devices) is displayed in green and orange. From this we can conclude that the observed upstream heating is not due to a redirection of bulk heating upon energizing of deflector gates. **a)** Upstream. **b)** Downstream

Supplement D: The Fractional Quantum Hall Edge at $\nu = 1$

The spatial separation between compressible edges is determined largely by the sharpness of the confining potential. At $\nu = 1$, the presence of FQH edge structure requires a shallow confining potential (compared to the magnetic length or Fermi wavelength), as well as a high mobility 2DES (as is always required for FQH physics). In this supplement, we will present data from an edge defined through a mesa etch, creating a steeper confining potential than what was presented in the main paper. As a result of the steeper confinement, we end up with edges of type III and IV (from Fig. 4) when the bulk is at $\nu = 1$. The gate-defined edge, as a reminder, had edges of type IV and V at bulk filling $\nu = 1$. From the table in Fig. 4, we can see that charge transport (R_{xy} and R_L) cannot discriminate between the type III and type IV edges. In this supplement, we will present evidence that both types of edge can exist in a single sample, and that they can be distinguished by monitoring upstream heat transport.

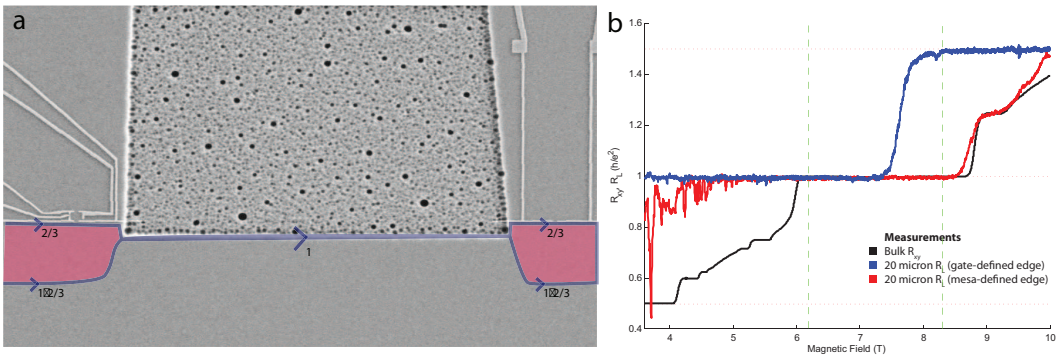

Figure S13: **a)** Modified device to study heat transport along a sharper edge. The gate defined edge (studied in the main paper) allowed for a $\nu = 2/3$ edge to form outside the $\nu = 1$ bulk (blue trace in panel **b**). The mesa-defined edge here is sharper, and the sharp density gradient may precludes FQH edge structure outside the $\nu = 1$ bulk. This image is of a device with 40 μm between heater and thermometer, while the device measured had 20 μm between heater and thermometer, to match the device presented in the main paper. **b)** R_L (red) for the device in panel **a**. The reduced resistance of the edge (red versus blue) at 8.3 T when switching from a gate-defined to a mesa-defined edge suggests that the originally separated FQH ($\nu = 2/3$ and $\nu = 1 \rightarrow 2/3$) channels are brought close together, allowing charge to equilibrate between them. While the device is drawn with an edge of type III (from Fig. 4 of the main paper), an edge of type IV cannot be ruled out from charge transport, either locally (R_L) or globally (R_{xy}).

In Figure S13, we present an SEM image of the device under consideration. The device geometry and substrate used are identical to those used for the device presented in the main paper. Using a wet-etching procedure, we are able to remove material between the QPC heater and the QD thermometer. This creates a physical boundary to the sample along which the edge propagates. The density in the 2DES must drop to zero across this edge, which can be happen over a shorter length scale than for an edge created by depleting the 2DES via electrostatic gating.

To demonstrate that this edge is sharper, we can repeat our local charge transport measurements (Fig. S13b, R_L in red). The observed enhanced conductance at any given field (red compared to blue) is a result of either more edges participating in transport, or a greater conductance of those edges participating. This is precisely what is expected if the edges are confined with a steeper potential. Here we will focus on behavior on the edge of the $\nu = 1$ bulk (6.2 T and 8.3 T). From the charge transport measurements, we cannot distinguish the exact edge structure at either field (see edges III and IV in Fig. 4).

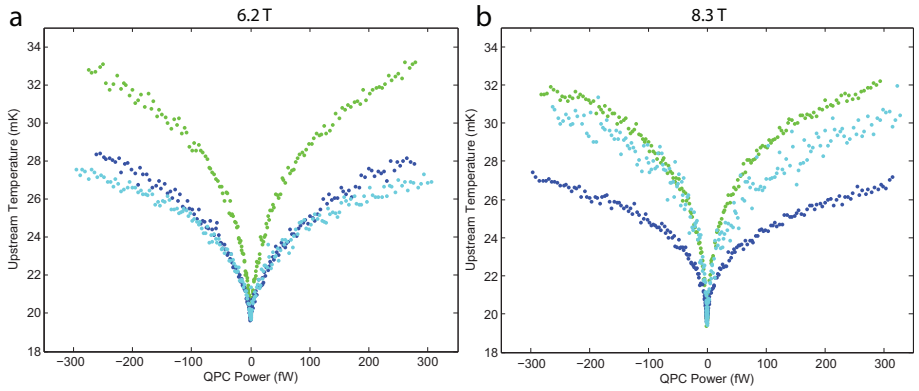

Figure S14: Upstream thermometry to identify FQH structure in the $\nu = 1$ edge. Dark blue curves depict background upstream heating, which we attribute to the bulk. The green curve depicts the heat observed with a gate-defined edge connecting heater and thermometer. The light blue curve depicts upstream heat observed with a sharper mesa-defined edge connecting heater and thermometer. **a)** At low fields, the upstream heating from the mesa-defined edge closely matches the background, suggesting no excess heat is carried by the edge. **b)** At high fields, there is a similar amount of upstream heating by both sharp and shallow edges, both appreciably above the background.

To distinguish between these two possible edge structures, we can perform upstream thermometry measurements. Because we have created our edge via etching the mesa, we cannot control for bulk heating by energizing and deenergizing deflection gates. However, by using an identical geometry to the gate-defined device, we can still identify the presence or absence of excess heat due to the edge. This thermometry measurement is presented in Fig. S14, with data from the edge-defined device in light blue. For comparison, data from the gate-defined device taken at the same fields is reproduced in dark blue and green (identical to upstream data in columns III and IV of Fig. 3 in the main paper).

At 6.2 T, we see that the temperature detected upstream (light blue) closely matches the temperature associated with bulk heating in the original device (dark blue). This is consistent with no heat being transported by the edge. The lack of upstream heat carried by the edge allows us to classify it as a simple IQH $\nu = 1$ edge (type III in Fig. 4), similar to what was observed at bulk fillings of $\nu = 2$ and $\nu = 3$ in the original device.

At 8.3 T, the temperature measured upstream (light blue in Fig. S14b) appears to be elevated, closely matching the temperature seen when a $\nu = 2/3$ edge connects the heater to the upstream thermometer in the original device (green curve). Recall that in the original device, this $\nu = 2/3$ edge was detectable via measurement of R_L (blue curve in Fig. 2). Here the charge signature has vanished ($R_L = R_{xy}$), but the nearly identical upstream heating strongly suggests that the $\nu = 2/3$ edge is still present (edge IV in Fig. 4). These measurements increase our confidence in assigning edge IV to our observations at 6.2 T in the original device.